arXiv:1303.1539v1 [cond-mat.supr-con] 6 Mar 2013

Majorana zero modes in dislocations of $\mathrm{Sr_2RuO_4}$

Taylor L. Hughes,[1] Hong Yao,[2] and Xiao-Liang Qi[3]

[1]*Department of Physics, University of Illinois at Urbana-Champaign, Urbana IL 61801, USA*
[2]*Institute for Advanced Study, Tsinghua University, Beijing, 100084, China*
[3]*Department of Physics, Stanford University, Stanford, CA 94305, USA*

(Dated: March 8, 2013)

We study the topologically protected Majorana zero modes induced by lattice dislocations in chiral topological superconductors. Dislocations provide a new way to realize Majorana zero modes at zero magnetic field. In particular, we study several different types of dislocations in the candidate material $\mathrm{Sr_2RuO_4}$. We also discuss the properties of linked dislocation lines and linked dislocation and flux lines. Various experimental consequences are predicted which provide a new approach to determine whether nature of the superconducting phase of $\mathrm{Sr_2RuO_4}$.

Introduction: Chiral topological superconductors (TSC) in 2D have garnered much attention over the past decade after the prediction that vortices in these superconducting phases harbor bound Majorana zero-modes[1]. This property is an important feature for topological quantum computing architectures which are based on the use of such non-Abelian anyon qubits[2, 3]. It is generally agreed that $\mathrm{Sr_2RuO_4}$ is a quasi-2D, p-wave superconductor with broken time-reversal symmetry, although the precise nature of the order parameter is still controversial (for a review, see Ref. [4]). So, while there is no concrete evidence that $\mathrm{Sr_2RuO_4}$ is a topological superconductor, it is one of the best candidate chiral topological superconductor materials.

The low-energy electronic structure of the normal metal state of $\mathrm{Sr_2RuO_4}$ is controlled by the t_{2g} multiplet of d-orbitals d_{xz}, d_{yz}, and d_{xy}. These three orbitals give rise to three Fermi-surfaces which are expected to become fully gapped below the superconducting transition temperature at $T_c \sim 1.5K$. The conventional wisdom indicates that the quasi-2D d_{xy} band dominates the pairing instability and develops a nodeless chiral $p_x + ip_y$ order parameter[5]. If such an order parameter were generated, then the recently measured half-quantum vortices would indeed bind Majorana fermion states[6, 7] which could be manipulated as qubits. On the other hand, a conflict between the theoretical prediction of chiral surface states in the $p_x + ip_y$ state, and the clear lack of surface currents measured in Ref. [8], motivated Raghu, Kapitulnik, and Kivelson (RKK) to make a different, compelling proposal for the nature of the order parameter which is dominated instead by the quasi-1D d_{xz} and d_{yz} orbitals[9]. The RKK order parameter is again, odd-parity/p-wave which breaks time-reversal, but it is not a chiral topological superconductor and should not exhibit chiral edge states. Thus, it is consistent with the measurements of Ref. [8]. The true nature of the order parameter is still an open question, and in light of this one seeks experiments that can distinguish between these two theories.

In this Letter we propose new experiments that can distinguish the two pairing schemes and also provide a new approach to Majorana zero modes. Our key observation is that the RKK order parameter, while trivial in the sense of 2D chiral superconductor, in fact is still nontrivial as a *weak* topological superconductor. Weak topological superconductors (and insulators)[10–13] are topological states protected by translation symmetry. They are distinguished by a topological invariant defined in a lower-dimensional sub-manifold of the Brillouin zone (BZ) (recall that the so-called *strong* invariant depends on the electronic structure in the entire BZ). For example, the 3D weak topological insulators are classified by three Z_2 invariants, which characterize whether the gapped Bloch Hamiltonian restricted to the three 2D planes of $k_x = \pi, k_y = \pi, k_z = \pi$ in the BZ are trivial or quantum spin Hall insulators in that plane. Heuristically, a non-trivial weak invariant indicates a state which is made from stacking up topological states of lower dimensions. Another example is a 2D superconductor in class D (no symmetry) which has two weak Z_2 indices. These exist since there is a strong Z_2 topological superconductor in this class in 1-dimension –the Majorana chain/p-wave wire[13–15]. We show that the RKK pairing of d_{xz} and d_{yz} bands corresponds to this type of weak topological superconductor. As a consequence, we show that naturally occurring or fabricated crystal defects exhibit a number of remarkable properties that are not shared by the conventional $p_x + ip_y$ state. These properties are not only useful for a characterization of the superconducting state but may have applications in quantum computing since, as we will show, these defects can trap Majorana zero modes.

3D *weak* topological superconductors: The non-interacting topological insulators and superconductors in generic dimensions have been classified[13, 15, 16]. Here we are interested in superconductors of class D (without time-reversal or spin-rotation symmetry), which have a strong Z_2 topological classification in 1D, Z in 2D, and trivial in 3D. For class D SCs in 3D with translational symmetries we can define weak topological invariants as well—the Chern numbers (which are defined in 2D) can be defined along constant k_x, k_y or k_z planes in the BZ. In a gapped state the Chern number cannot change, so the Chern number in different $k_z = \mathrm{const}$ planes is the same integer n_z. Similarly n_x and n_y can be defined for the other two planes, as is illustrated in Fig. 1(a). The integer-valued vector $\mathbf{n} = (n_x, n_y, n_z)$ are the *primary weak indices* of the 3D TSC. A system with indices $\mathbf{n}$ is *topologically* equivalent to a set of decoupled 2D layers of topological chiral superconductors with non-vanishing Chern number,

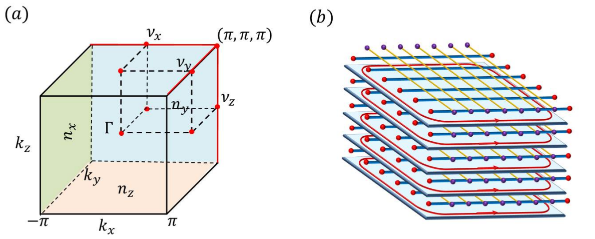

FIG. 1. (a) The Brillouin zone of a 3D SC. The primary weak topological invariants $\mathbf{n} = (n_x, n_y, n_z)$ are defined as the Chern numbers in the three independent planes (colored green, blue and red), and the secondary weak topological invariants $\boldsymbol{\nu} = (\nu_x, \nu_y, \nu_z)$ are defined as the 1D Z_2 indices along the three perpendicular lines colored in red. (b) Illustration that a topological superconductor with topological invariants $\mathbf{n} = (0, 0, 1)$, $\boldsymbol{\nu} = (1, 1, 0)$, such as $\mathrm{Sr_2RuO_4}$ (see text) is equivalent to decoupled layers of chiral superconductors (with the red line and arrow labeling the chiral edge states) and 1D wires along x and y directions with Majorana zero modes at end points.

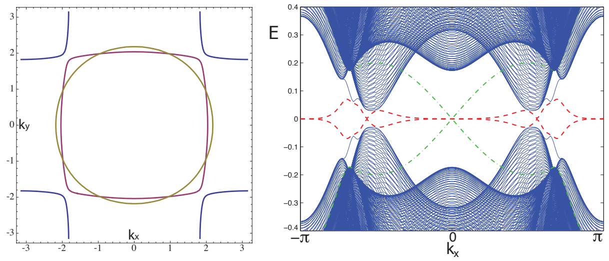

FIG. 2. (Left panel) Fermi-surface structure of $\mathrm{Sr_2RuO_4}$ showing the Fermi surfaces coming from the d_{xz} d_{yz} and d_{xy} bands with orbital mixing. (Right panel) Low-energy quasi-particle spectrum of superconducting $\mathrm{Sr_2RuO_4}$ for a geometry with open boundary conditions in the y-direction and periodic boundary conditions on the x-direction. The states in red-dashed lines are edge states arising from the quasi-1D bands; notice they exist at $k_x = 0$ and $k_x = \pi$. The green dash-dotted lines are the edge states arising from the quasi-2D band; notice they exist only around $k_x = 0$.

stacked along the $\mathbf{n}$ direction. For any surface plane which is not perpendicular to $\mathbf{n}$, there will be chiral surface states.

Similarly, the 1D Z_2 invariants[14] can be calculated along time-reversal invariant lines in the 3D BZ[17]. The three *secondary weak topological invariants* are defined as the Z_2 invariants along the three lines $(k_y, k_z) = (\pi, \pi)$, $(k_z, k_x) = (\pi, \pi)$, $(k_x, k_y) = (\pi, \pi)$. We collect them into a vector $\boldsymbol{\nu} = (\nu_x, \nu_y, \nu_z)$ shown in Fig. 1 (a) (with $\nu_{x,y,z} = 0, 1$). It can be shown that $\boldsymbol{\nu}$ and $\mathbf{n}$ together determine the Z_2 invariant along all other time-reversal invariant lines. A TSC with $\boldsymbol{\nu} \neq 0$ and $\mathbf{n} = 0$ is *topologically* equivalent to decoupled 1D topological superconductor wires aligned in the direction of $\boldsymbol{\nu}$, each of which has Majorana zero modes at the end. Consequently, for any surface plane that is not *parallel* to ν there will be Majorana surface states on that surface. A generic TSC with both $\mathbf{n}$ and $\boldsymbol{\nu}$ non-vanishing can be considered as decoupled layers of 2D chiral TSC coexisting with decoupled wires of 1D TSC. For example, we will show later that the RKK model of $\mathrm{Sr_2RuO_4}$ (with the additional spin degeneracy ignored) has the weak topological invariants $\mathbf{n} = (0, 0, 1)$, $\boldsymbol{\nu} = (1, 1, 0)$, which is equivalent to decoupled layers and wires as is illustrated in Fig. 1 (b). This conceptual decomposition into stacks of lower dimensional systems will be helpful to illustrate our later discussion of dislocation properties. Primary weak topological indices were first discussed in the context of time-reversal invariant topological insulators[10, 11, 18] and subsequently both primary and secondary indices (and beyond) can be straightforwardly extracted for the entire periodic table of topological insulators and superconductors from the K-theory calculation in Ref. 13. We briefly remark that although we have defined the secondary-index $\boldsymbol{\nu}$ as a vector the natural structure is actually an anti-symmetric two-index tensor which can be interpreted as a vector only in 3D.[19, 20]

Application in $\mathrm{Sr_2RuO_4}$: We will now discuss the electronic structure of the normal metal state of $\mathrm{Sr_2RuO_4}$ followed by the superconducting pairing scheme as given in the paper by RKK[9]. The three relevant orbitals for the electronic structure are the t_{2g} multiplet d_{xz}, d_{yz}, d_{xy} which will be labelled by $\alpha = 1, 2, 3$. The layered structure of $\mathrm{Sr_2RuO_4}$ makes the system behave quasi-two dimensionally; consequently the first two orbitals are effectively quasi-1D in nature while d_{xy} is quasi-2D. The bandstructure can be modeled using these three orbitals, plus spin, on a simple tetragonal lattice with nearest neighbor, and next-nearest neighbor hoppings. The Bloch Hamiltonian, without spin-orbit coupling, is

$$H(\mathbf{k}) = \begin{pmatrix} \epsilon_{xz}(\mathbf{k}) & \Lambda(\mathbf{k}) & 0 \\ \Lambda(\mathbf{k}) & \epsilon_{yz}(\mathbf{k}) & 0 \\ 0 & 0 & \epsilon_{xy}(\mathbf{k}) \end{pmatrix} \otimes \mathbb{I}_{spin} \qquad (1)$$

$$\begin{aligned} \epsilon_{xz}(\mathbf{k}) &= -2t\cos k_x - 2t^{\perp}\cos k_y - 2t_1^z \cos k_z \\ \epsilon_{yz}(\mathbf{k}) &= -2t\cos k_y - 2t^{\perp}\cos k_x - 2t_1^z \cos k_z \\ \epsilon_{xy}(\mathbf{k}) &= -2t'(\cos k_x + \cos k_y) - 4t''\cos k_x \cos k_y - 2t_2^z \cos k_z \\ \Lambda(\mathbf{k}) &= -2\lambda \sin k_x \sin k_y \end{aligned}$$

where values of in-plane hopping parameters taken from RKK are $t = 1.0, t' = 0.8, t^{\perp} = 0.1, t'' = 0.3$. We have also considered an orbital-hybridization term $\Lambda(\mathbf{k})$ which arises from next-nearest neighbor hopping between different quasi-1D orbitals in xy plane and which removes the crossings of Fermi surfaces of quasi-1D orbitals. Hopping amplitudes along z are t_1^z and t_2^z for quasi-1D and quasi-2D orbitals, respectively. Due to the layered structure of the lattice, out-of-plane hoppings are negligibly small[21, 22] and we shall consider the 2D limit hereafter. In Fig. 2 we show the Fermi-surfaces due to these orbitals. There are three Fermi-surfaces: two around $(k_x, k_y) = (0, 0)$ and one around $(k_x, k_y) = (\pi, \pi)$. The two quasi-1D Fermi-surfaces from d_{xz} and d_{yz} orbitals do not touch as long as $\lambda \neq 0$. The inner quasi-1D Fermi-surface is a hole pocket, and the outer Fermi-surface is an electron-pocket. The round quasi-2D Fermi-surface arises from the d_{xy} orbital which we assume is completely decoupled in the 2D limit[23].

We now want to consider the properties of the superconducting state of $\mathrm{Sr_2RuO_4}$. For the quasi-2D band we assume triplet p_x+ip_y pairing. For values of the Fermi-level which lie within the quasi-2D band (which is expected in experiments) this would mean that the system will be a weak 3D topological superconductor with primary index $\mathbf{n}=(0,0,1)$. For the quasi-1D bands we assume the RKK pairing which we now describe. Since the quasi-1D and quasi-2D orbitals are assumed to be approximately decoupled we can write a reduced two-orbital model for the quasi-1D orbitals:

$$H(\mathbf{k})=\begin{pmatrix}\epsilon_{xz}(\mathbf{k}) & \Lambda(\mathbf{k})\\ \Lambda(\mathbf{k}) & \epsilon_{yz}(\mathbf{k})\end{pmatrix}\otimes\mathbb{I}_{spin} \tag{2}$$

with $\lambda=0.1t$. The superconducting pairing that RKK propose is spin-triplet and intra-orbital. The pairing functions of orbital α for this chiral superconducting state are

$$\Delta_\alpha = i\mathbf{d}_\alpha(\mathbf{k})\cdot\vec{\sigma}\sigma^y,\quad \alpha=1,2 \tag{3}$$

$$\mathbf{d}_1 = \hat{z}\Delta_0\sin k_x\cos k_y, \tag{4}$$

$$\mathbf{d}_2 = i\hat{z}\Delta_0\sin k_y\cos k_x, \tag{5}$$

where the direction of $\mathbf{d}_\alpha$ and the relative phase between $\mathbf{d}_1$ and $\mathbf{d}_2$ are determined by the small spin-orbit coupling. The superconducting pairing winds around the two Fermi surfaces with the same chirality, but since they have the opposite charge character they contribute oppositely to the winding number yielding a vanishing Chern number. However, in a clean system there should be edge states located near $k_x=0$ and $k_x=\pi$ if, for example we put the system on a cylinder with open boundary conditions in the y-direction and periodic boundary conditions in the x-direction. The energy spectrum for such a system is shown in Fig. 2 with clear low-energy modes near $k_x=0,\pi$ which develop zero modes exactly at these k-points. These edge states exist because of a non-trivial secondary weak index $\boldsymbol{\nu}=(1,1,0)$ due to the RKK pairing. Even though n, and other quantities, should be doubled when the spin degeneracy is taken into account, it has no qualitative effect on most of the properties of lattice dislocations we discuss below when the effects of spin-orbit coupling are weak. We defer the discussions of strong spin-orbit coupling to future work.

Properties of dislocations and linked dislocation lines: In addition to the surface state properties, weak topological indices have profound consequences for the properties of crystal defects such as dislocations[19, 20, 24]. For the 3D crystal we are considering, a lattice dislocation is a line defect around which the ions are displaced by an integer-valued vector $\mathbf{b}$ in the lattice vector basis, which is known as the Burgers vector. A dislocation is described by $\mathbf{b}$ and another integer-valued vector, the tangent vector of the dislocation $\mathbf{l}$. The relative orientation of $\mathbf{b}$ and $\mathbf{l}$ determines the type of dislocation: edge ($\mathbf{l}\cdot\mathbf{b}=0$), screw ($\mathbf{l}$ parallel to $\mathbf{b}$), and mixed ($\mathbf{l}$ neither parallel nor perpendicular to $\mathbf{b}$). While $\mathbf{b}$ is a topological property of a dislocation line, $\mathbf{l}$ (namely the dislocation-type) is not.

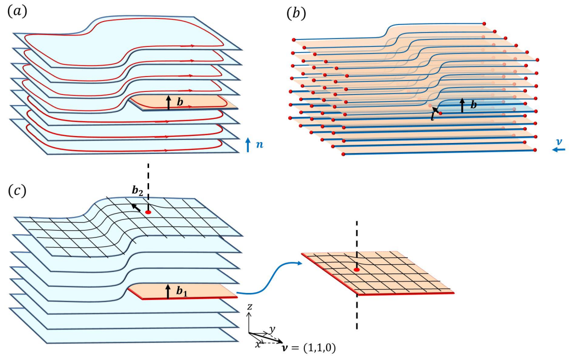

FIG. 3. (a) Illustration of an edge dislocation line with Burgers vector $\mathbf{b}$ in a TSC consisting of decoupled layers stacked along the direction of topological index vector $\mathbf{n}$. (b) Illustration of an edge dislocation line with Burgest vector $\mathbf{b}$ and direction $\mathbf{l}$ in a TSC consisting of decoupled 1D wires along the direction of secondary weak topological index vector $\boldsymbol{\nu}$. The red dots at the end of wires represent Majorana zero modes.(c) Illustration of the Majorana zero modes induced by linking of two edge dislocations with $\mathbf{b}_1=\hat{z}$ and $\mathbf{b}_2=-\hat{x}$ in the decoupled plane limit.There is a Majorana zero mode at each dislocation line, indicated by the red dot and red line.

Both the primary and secondary weak topological indices can be probed by dislocations. The primary weak indices $\mathbf{n}$ lead to $N_1=\mathbf{n}\cdot\mathbf{b}$ number of chiral Majorana modes propagating along the dislocation[19]. Note that N_1 is independent of the dislocation direction $\mathbf{l}$ and thus topological. The sign of the integer N_1 determines the chirality of the edge state, which is defined with respect to $\mathbf{l}$. This fact can be easily understood for an edge dislocation with $\mathbf{n}$ perpendicular to $\mathbf{l}$, in which case the dislocation can be obtained by adding an additional layer of chiral 2D TSC to one side of the dislocation line, as is illustrated in Fig. 3 (a). The secondary weak indices $\boldsymbol{\nu}$ lead to non-chiral 1D Majorana modes if $N_2=(\mathbf{b}\times\mathbf{l})\cdot\boldsymbol{\nu}=1$ mod 2. The modes determined by N_2 are like the "weak" analog of the "strong" modes determined by N_1. The dependence of N_2 on the variable direction $\mathbf{l}$ indicates that topological stability will require an additional symmetry which in this case is translation symmetry along the dislocation (*i.e.* the direction $\mathbf{l}$ cannot change along the dislocation line). The non-chiral Majorana propagating modes are protected by translation symmetry along the dislocation, since its left and right moving branches are around the 1D momenta 0 and π, which cannot be coupled without breaking translation symmetry. Also we see that N_2 is nontrivial only for edge dislocations with $\mathbf{b}\times\mathbf{l}\neq 0$. In the topologically equivalent decoupled chain limit (which is appropriate for a system with $\boldsymbol{\nu}\neq 0$) the dislocation bound states can be understood intuitively, as is illustrated in Fig. 3 (b). Decoupled 1D Majorana chains along the $\boldsymbol{\nu}$ direction terminate at the dislocation line and the Majorana zero modes at their end points couple to form the 1D non-chiral Majorana edge state. It is thus intuitive to take N_1 to be akin to a "strong" *dislocation* invariant and N_2 to be a "weak" *dislocation* invariant.

One additional effect that has thus far gone unnoticed is the property of closed dislocation lines which are linked, *i.e.*, dislocation rings. Along a finite-length dislocation ring with nontrivial topological invariants N_1 and/or N_2, the Majorana fermion energy spectrum becomes discrete, and the boundary condition around the ring determines whether there is an exact Majorana zero mode at zero energy. Interestingly, the boundary condition around a dislocation ring depends on its linking with other dislocation rings and with flux/vortex lines. To illustrate this effect, consider the RKK model with $\boldsymbol{\nu} = (1, 1, 0)$ and consider two edge dislocation lines. The first one has $\mathbf{b}_1 = (1, 0, 0)$ and is straight along the $\hat{z}$ direction so that $\mathbf{l} = \hat{z}$. The second one is a circle in the xy plane with $\mathbf{b}_2 = (0, 0, 1)$. If these two dislocations are not linked, the Majorana fermion mode along the in-plane dislocation has a finite size gap with no exact zero mode. This can be understood easily in the decoupled-layer limit shown in Fig. 3(c), in which case the in-plane dislocation circle is the boundary of a single-layer disk, and a finite gap of order $1/R$ (with R the radius of the circle) is present. In contrast, when the circle encloses the other dislocation line along $\hat{z}$ direction, in the decoupled layer limit the effect is to introduce an edge dislocation with Burgers vector $\mathbf{b}_1$ in the disk, which introduces an additional Majorana zero mode at the dislocation line. Since Majorana zero modes have to come in pairs, there must also be a Majorana zero mode around the other dislocation with circular shape[25]. Since any generic superconductors can be deformed to the decoupled layer limit (due to the absence of strong invariant in 3D), the number of Majorana zero modes on linking dislocations can be determined only from investigating the decoupled layer limit, which gives the number of Majorana zero modes to be $N_0 = N_L \left(\mathbf{b}_1 \times \mathbf{b}_2\right) \cdot \boldsymbol{\nu}$ mod 2, with N_L the linking number of the two edge dislocations. We note that the dependence on $\mathbf{l}$ has dropped out which means that N_0 is topological and does not require the addition of translation symmetry along the dislocations. Thus we see that a primary consequence of the secondary weak invariant is the determination of bound states on linked dislocations. If we had left $\boldsymbol{\nu}$ as an anti-symmetric tensor this invariant would simply be the contraction of the tensor with the Burgers' vectors of both dislocation lines.

While the primary weak invariant N_1 has no effect in the linking of two dislocations, it does determine the Majorana zero modes when linking occurs between dislocation lines and flux/vortex lines. Obviously when a superconducting vortex ring is linked with a dislocation ring, the boundary condition for the Majorana fermion along the dislocation will change. For odd N_1 such a boundary condition change results in a single Majorana zero mode on the dislocation line, and another one on the vortex line. The exitance of Majorana mode on the dislocation line is determined by $\tilde{N}_0 = \tilde{N}_L N_1$ mod 2, where $\tilde{N}_L$ is the linking number between a dislocation line and a vortex line.

Physical consequences: Before we conclude, we now discuss a few measurable experimental consequences of the predicted Majorana fermions bound to dislocations:

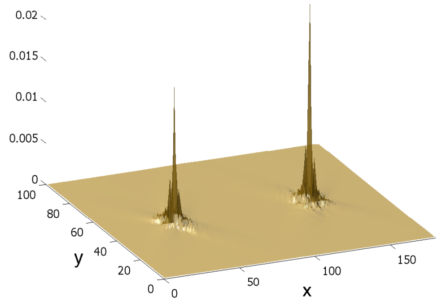

FIG. 4. Spatial profile of the lowest energy bound state that is bound to the ends of a dislocation that stretches from $x = 40$ to $x = 120$ on the line $y = 50$. The total lattice size is 160×100. The asymmetry in the density profile is due to finite-size error introduced by discretization.

1) The one-dimensional Majorana modes have a constant density of states. Consequently, it contributes a specific heat C_V that is linear in temperature, and is proportional to the density of dislocations[26]. Since the dislocations in a $\mathrm{Sr_2RuO_4}$ sample can be observed by transmission electron microscopy (TEM)[27], measuring samples with different dislocation density can verify whether C_V/T in the low temperature limit is indeed proportional to the dislocation density.

2) Due to the nontrivial primary weak topological invariant $\mathbf{n}$, the dislocations with Burgers vector $\mathbf{b} = \hat{z}$ have chiral Majorana fermion modes. Thus, each such dislocation carries a chiral heat current $I_E = \frac{\pi k_B^2 T^2}{24\hbar}$[28] along the dislocation line. With a random distribution of dislocations in the system, the flow direction of the chiral heat current is also random, so that a net chiral heat flow will not be observed. However, the chiral heat current along random dislocations will contribute a thermal conductivity that is proportional to the dislocation density. Furthermore, it is possible to have a system with imbalanced dislocation lines. For example, in a system with a uniaxial strain $u_{zz}(y)$ that has a gradient along the y-direction, it is preferred to have edge dislocations along the x-direction with more Burgers vector $\mathbf{b} = +\hat{z}$ than $\mathbf{b} = -\hat{z}$. If the density of the $\mathbf{b} = +\hat{z}$ ($\mathbf{b} = -\hat{z}$) edge dislocations are ρ_+ (ρ_-) respectively, there will be a chiral heat current density $j_E = \left(\rho_+ - \rho_-\right) \frac{\pi k_B^2 T^2}{24\hbar}$. Compared to the thermal current carried by the edge states which is easily overwhelmed by bulk thermal conduction, the dislocation current can be a bulk effect that remains finite in the thermodynamic limit.

3) If there is an edge dislocation ring in the xy-plane (with Burgers vector $\mathbf{b}_1 = \hat{z}$) and a second edge dislocation along the z-axis threading the ring (with Burgers vector $\mathbf{b}_2$ in-plane), then the Majorana zero mode in the second dislocation may be observable by scanning tunneling microscopy (STM). In particular, when the first dislocation is at a crystal surface, it will be a disk-shaped plateau on the surface, threaded by the second dislocation line and be easy to locate using, for example, TEM.

Acknowledgement: We thank S. A. Kivelson, Y. Liu, A.

Mackenzie and S. Raghu for helpful discussions. This work is supported in part by the US Department of Energy under contract DE-FG02-07ER46453 (TLH), the Tsinghua Startup Funds and the National Thousand Young Talents Program of China (HY), and the National Science Foundation through the grant No. DMR-1151786 (XLQ). TLH also thanks the support of the ICMT at UIUC. After the completion of this work we noticed a recent preprint with similar themes albeit a different focus[29].

[1] N. Read and D. Green, Phys. Rev. B **61**, 10267 (2000).
[2] A. Y. Kitaev, Ann. Phys. (N.Y.) **303**, 2 (2003).
[3] C. Nayak, S. H. Simon, A. Stern, M. Freedman, and S. D. Sarma, Rev. Mod. Phys. **80**, 1083 (2008).
[4] C. Kallin, Reports on Progress in Physics **75**, 042501 (2012).
[5] T. M. Rice and M. Sigrist, J. Phys.: Condens. Matter **7**, L643 (1995).
[6] See A. J. Leggett, Rev. Mod. Phys. **47** 331 (1975), and references therein.
[7] J. Jang, D. G. Ferguson, V. Vakaryuk, R. Budakian, S. B. Chung, P. M. Goldbart, and Y. Maeno, Science **331**, 186 (2011).
[8] P. G. Björnsson, Y. Maeno, M. E. Huber, and K. A. Moler, Phys. Rev. B **72**, 012504 (2005).
[9] S. Raghu, A. Kapitulnik, and S. A. Kivelson, Phys. Rev. Lett. **105**, 136401 (2010).
[10] L. Fu, C. L. Kane, and E. J. Mele, Phys. Rev. Lett. **98**, 106803 (2007).
[11] J. E. Moore and L. Balents, Phys. Rev. B **75**, 121306 (2007).
[12] R. Roy, Phys. Rev. B **79**, 195322 (2009).
[13] A. Kitaev, AIP Conf. Proc. **1134**, 22 (2009).
[14] A. Y. Kitaev, Physics-Uspekhi **44**, 131 (2001).
[15] A. P. Schnyder, S. Ryu, A. Furusaki, and A. W. W. Ludwig, Phys. Rev. B **78**, 195125 (2008).
[16] X.-L. Qi, T. Hughes, and S.-C. Zhang, Phys. Rev. B **78**, 195424 (2008).
[17] The 1D Z_2 topological invariants are defined only when the particle-hole symmetry is respected, which is guaranteed along time-reversal invariant lines in the 3D BZ.
[18] R. Roy, Phys. Rev. B **79**, 195321 (2009).
[19] Y. Ran, arXiv:1006.5454 (2010).
[20] J. C. Teo and C. L. Kane, Physical Review B **82**, 115120 (2010).
[21] A. P. Mackenzie, S. R. Julian, A. J. Diver, G. J. McMullan, M. P. Ray, G. G. Lonzarich, Y. Maeno, S. Nishizaki, and T. Fujita, Phys. Rev. Lett. **76**, 3786 (1996).
[22] A. Damascelli, D. H. Lu, K. M. Shen, N. P. Armitage, F. Ronning, D. L. Feng, C. Kim, Z.-X. Shen, T. Kimura, Y. Tokura, Z. Q. Mao, and Y. Maeno, Phys. Rev. Lett. **85**, 5194 (2000).
[23] Weak hybridization between quasi-2D and quasi-1D orbitals would occur when out-of-plane hoppings are considered.
[24] Y. Ran, Y. Zhang, and A. Vishwanath, Nature Phys. **5**, 298 (2009).
[25] Couplings between two Majorana zero-modes can only generate a exponentially small gap of order of $e^{-R/\xi}$, where ξ is the correlation length of the superconductor.
[26] Early specific heat measurement has reported evidences of residual gapless excitations at low temperature[30].
[27] Y. Ying, N. Staley, Y. Xin, K. Sun, X. Cai, D. Fobes, T. Liu, Z. Mao, and Y. Liu, arXiv preprint arXiv:1205.3250 (2012).
[28] C. L. Kane and M. P. A. Fisher, Phys. Rev. B **55**, 15832 (1997).
[29] Y. Ueno, A. Yamakage, Y. Tanaka, and M. Sato, "Symmetry-protected majorana fermions in superconductors: Theory and application to sr2ruo4," arxiv:1303.0202 (2013).
[30] S. NishiZaki, Y. Maeno, and Z. Mao, J. Phys. Soc. Jpn. **69**, 572 (2000).